Theoretical and simulation studies of recombinative temperature programmed desorption

B. Meng and W. H. Weinberg
Department of Chemical Engineering, University of California, Santa Barbara, California 93106

(Received 20 June 1994; accepted 5 October 1994)

Using Monte Carlo simulations and both quasichemical (for nearest neighbors) and mean field (for next-nearest neighbors) approximations, we explore a kinetic lattice gas model to investigate recombinative thermal desorption. A previously introduced Monte Carlo algorithm, which correctly relates Monte Carlo simulation time and real time, is extended in order to quantify the kinetics and energetics of recombinative thermal desorption spectra. We consider the effects of lateral interactions between adsorbates, lattice geometry, and limited mobility of the adsorbate (nonequilibrium) on the temperature programmed desorption spectra. Furthermore, we analyze the apparent coverage dependence of both the activation energy and the preexponential factor of the desorption rate coefficient for both repulsive and attractive nearest-neighbor interactions on a square lattice. For a repulsive nearest-neighbor interaction, we find that kinetic compensation occurs for a surface coverage less than 0.6. However, for surface coverages greater than 0.6, we find that the activation energy and preexponential factor do not vary sympathetically. For an attractive nearest-neighbor interaction, kinetic compensation is only observed at high coverage. We elucidate the compensation effect quantitatively by considering the configurational distribution of adsorbates. © *1995 American Institute of Physics.*

I. INTRODUCTION

Temperature programmed desorption (TPD) has been the most widely used experimental technique for the investigation of interaction energies between an adsorbate and a surface. The interpretation of TPD spectra has usually been carried out using the simple Arrhenius equation with the rate coefficient of desorption expressed in the Polanyi–Wigner form,[1–8] namely,

$$R_d = k_d^{(0)} \exp(-E_d/k_B T)\,\theta_A^n, \tag{1}$$

where R_d is the rate of desorption, $k_d^{(0)}$ and E_d are the preexponential factor and the activation energy of the desorption rate coefficient, T is the surface temperature, θ_A is the fractional surface coverage of the adsorbate, and n is the order of the desorption reaction. In the presence of adsorbate–adsorbate interactions, the activation energy and the preexponential factor may vary (and vary nonlinearly) with the surface coverage of adsorbate.[9]

Assuming that the adsorbate is distributed on a reactive lattice commensurate with the substrate surface, the kinetics of desorption can be described by a lattice gas model. Although a simple expression can be constructed for the desorption rate using the lattice gas model, it cannot be solved exactly except in some special cases.[10] Therefore, mean field[11] and quasichemical approximations,[12–19] a combination of these two approximations,[20] transfer matrix techniques,[21–24] and other analytical methods[25–28] have been introduced to take into account lateral interactions between adsorbates. Since exact results of the lattice gas model can be derived using Monte Carlo simulations (at least in principle), this technique has now been used extensively to study the kinetics of desorption.[29–45] From Monte Carlo simulations, we can also directly map the configurational changes of the adsorbate during desorption. Furthermore, we can easily study adsorbate phase transformations as a function of surface coverage and temperature, which may be correlated with experimental LEED and STM observations, for example.

In this paper, we extend the Monte Carlo algorithm we have previously introduced[46] to simulate recombinative TPD spectra with the correct connection between Monte Carlo simulation time and real time. Unlike Monte Carlo algorithms employed previously,[39–43] the time increment after a desorption event is calculated directly from the total desorption rate on the surface in our algorithm, with the proper relationship derived from the rate equation. The algorithm provides a convenient way to study isosteric properties for which the surface coverage must be monitored. Thermal desorption spectra are calculated both from Monte Carlo simulations and employing quasichemical and mean field approximations. We then discuss the effects on the TPD spectra of nearest-neighbor and next-nearest-neighbor interactions between adsorbates, the effects of the geometry of the substrate (triangular, square, and hexagonal lattices), and the (nonequilibrium) effects of limited mobility of the adsorbate. We also examine the behavior of the coverage-dependent activation energy and preexponential factor of the desorption rate coefficient for both repulsive and attractive nearest neighbor interactions on a square lattice.

II. MODEL AND ALGORITHM

In the lattice gas model, the surface is represented by a triangular, a square, or a hexagonal lattice of adsorption sites. These lattices are shown in Fig. 1 together with the nearest-neighbor (nn) and next-nearest-neighbor (nnn) lattice sites. Monte Carlo simulations of the model have been conducted on $(L \times L)$ lattices with periodic boundary conditions, where $L = 80$ lattice constants. Here, we consider recombinative de-

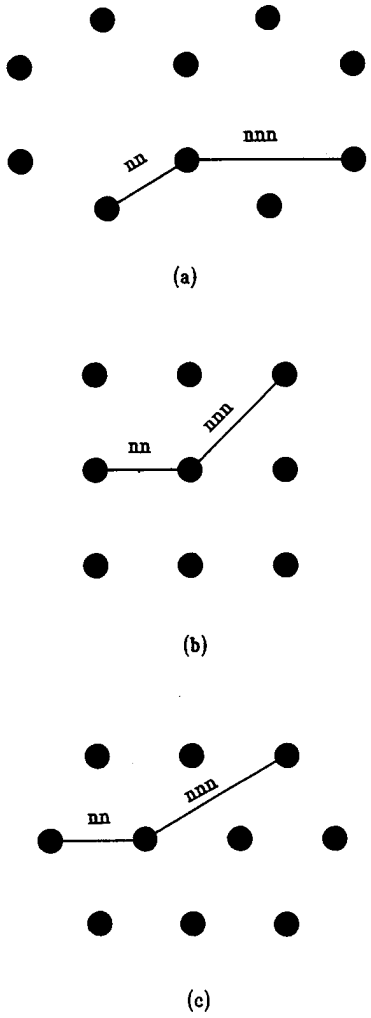

FIG. 1. Schematic of (a) triangular, (b) square, and (c) hexagonal lattices with nearest neighbors (nn) and next nearest neighbors (nnn) denoted explicitly.

sorption, i.e., second-order desorption, taking into account both nearest-neighbor and next-nearest-neighbor interactions. Considering all the different types of local configurations of the adsorbate on the surface, the desorption rate equation describing $2A(a)\rightarrow A_2(g)$ has the form

$$-d\theta_A/dt=\sum_i \theta_{AA,i}k_{d,i}^{(0)}\exp(-E_{d,i}/k_BT), \tag{2}$$

where $k_{d,i}^{(0)}$ is the preexponential factor of the desorption rate coefficient of a nearest-neighbor pair of adsorbates with local configuration of type i, $\theta_{AA,i}$ is the fractional coverage of a nearest-neighbor pair with local configuration of type i, and $E_{d,i}$ is the activation energy of desorption for a nearest-neighbor pair in a local configuration of type i, which we assume is given by

$$E_{d,i}=E_d(0)-N_{\rm nn}(i)E_{\rm nn}-N_{\rm nnn}(i)E_{\rm nnn}. \tag{3}$$

Here, $E_d(0)$ is the activation energy of desorption of an isolated nearest-neighbor pair. The quantities $N_{\rm nn}(i)$ and $N_{\rm nnn}(i)$ are the number of nearest neighbors and next nearest neighbors of the nearest-neighbor pair with local configuration of type i, and $E_{\rm nn}$ and $E_{\rm nnn}$ are the nearest-neighbor and next-nearest-neighbor interaction energies. In the simulations and the analytical calculations, we assume that the preexponential factor for all local configurations is constant and equal to $k_d^{(0)}$. More specifically, we choose $E_d(0)=30$ kcal/mol and $k_d^{(0)}=10^{15}$ s^{-1} in all of the simulations.

Equation (2) can also be expressed as

$$-dN_A/dt=(2/z)\sum_i N_{AA}(i)k_d^{(0)}\exp(-E_{d,i}/k_BT), \tag{4}$$

where $N_{AA}(i)$ is the number of nearest neighbors with local configuration of type i, and z is the number of nearest-neighbor sites. Therefore, the time increment for desorption of a nearest-neighbor pair from the surface is given by

$$\tau(N_A)=z\Big/\sum_i N_{AA}(i)k_d^{(0)}\exp(-E_{d,i}/k_BT). \tag{5}$$

Except where noted, we also assume that the rate of surface diffusion is much more rapid than that of desorption, i.e., the adsorbate is considered to be in a quasiequilibrium state.[47] This assumption is usually acceptable, especially for metallic surfaces for which the activation energy of surface diffusion is about 10–20% of the substrate-adsorbate bond energy.

The Monte Carlo algorithm is formulated as follows.

(1) Randomly populate N_0 adsorbate atoms on the $(L\times L)$ lattice at an initial coverage θ_0 $(=N_0/L^2)$.

(2) Relax the surface until a thermodynamic equilibrium distribution of the adsorbate is established. This redistribution of the adsorbate is carried out as follows. An adsorbate particle is chosen randomly (at, say, site i), and one of the z nearest-neighbor sites (site j) is also randomly chosen. If the jth site is occupied, an attempted hop fails, and the procedure is repeated. If the jth site is vacant, the particle hops into it from its original ith site with a probability $P_{i,j}$ $(=\exp[-(E_{d,j}-E_{d,i})/k_BT])$ if $E_{d,j}>E_{d,i}$, and with a probability of unity if $E_{d,j}\leqslant E_{d,i}$. The values of $E_{d,i}$ and $E_{d,j}$ are determined from Eq. (3). This procedure is repeated until an equilibrium distribution of the adsorbate on the surface is achieved.

(3) The desorption rate is calculated for each nearest-neighbor pair k from the following expression:

$$r_k=k_d^{(0)}\exp(-E_{d,k}/k_BT). \tag{6}$$

The pair of the adparticles that has the maximum desorption rate, $r_{\rm max}$, is identified and updated throughout the course of the simulation.

(4) A pair of adparticles of index k is chosen at random and desorbs with a probability P_k $(=r_k/r_{\rm max})$. If a desorption event is realized, time is updated by an increment

$$\tau(N_A)=z\Big/\sum_i N_{AA}(i)r_i. \tag{7}$$

The temperature is also updated after each desorption event by an increment $\beta\tau(N_A)$, where β is the chosen heating rate.

(5) Reestablish the surface to a new thermodynamic equilibrium distribution of adsorbates as in step 2.

(6) Repeat steps (3)–(5) until all adsorbed particles have desorbed.

The desorption rate in the time interval Δt is

$$R_d = \Delta N_A / (L^2 \Delta t), \tag{8}$$

where ΔN_A is the number of adsorbate particles which have desorbed in time Δt. It should be noted that this convention implies that the production rate of $A_2(g)$ is equal to $2R_d$.

III. GENERAL EQUATIONS FROM APPROXIMATE METHODS

Using the quasichemical approximation to describe nearest-neighbor interactions and a mean field approximation to describe next-nearest-neighbor interactions,[12,20] Eq. (2) can be expressed as

$$R_d = k_d^{(0)} \exp[-(E_0 - 2zE_{\mathrm{nnn}}\theta_A)/k_B T]\xi, \tag{9}$$

for the case of second-order desorption, where

$$\begin{aligned}
\xi &= \theta_{AA}\{[\theta_{AA} \exp(E_{\mathrm{nn}}/k_B T) + 0.5\theta_{AS}]/\theta_A\}^m, \\
\theta_{AA} &= \theta_A - \{1 - [1 - 2\alpha\theta_A(1-\theta_A)]^{1/2}\}/\alpha, \\
\theta_{AS} &= 2\{1 - [1 - 2\alpha\theta_A(1-\theta_A)]^{1/2}\}/\alpha, \\
\theta_{SS} &= 1 - \theta_A - \{1 - [1 - 2\alpha\theta_A(1-\theta_A)]^{1/2}\}/\alpha, \\
\alpha &= 2[1 - \exp(-E_{\mathrm{nn}}/k_B T)],
\end{aligned} \tag{10}$$

with $m = 2z - 2$ and $z = 3$, 4, and 6 for triangular, square, and hexagonal lattices, respectively. Here, a subscript A denotes an adsorbate particle, a subscript S denotes an unoccupied lattice site, and a subscript ij denotes a nearest-neighbor ij pair on the surface (where i and j are A or S).

IV. RESULTS AND DISCUSSION

In order to demonstrate our methodology, we first simulated second-order temperature programmed desorption spectra of a noninteracting lattice gas on a triangular lattice, a square lattice, and a hexagonal lattice. Good agreement between the Monte Carlo simulations and desorption spectra calculated using the appropriate continuum differential equation was achieved in all cases. For example, Fig. 2(a) shows the TPD spectra obtained from both Monte Carlo simulations and the continuum differential equation on a triangular lattice with initial coverages ranging from 0.25 to 1.0, and Fig. 2(b) is a representative configuration at a fractional surface coverage of 0.5 (parameter set A in Table I). Without lateral interactions, the adsorbate can be treated as randomly distributed on the surface, and the model reduces to one which is described by the continuum equation. Therefore, the two results should be the same, a conclusion which is verified by the desorption spectra of Fig. 2. Note that the lower signal-to-noise ratio in the Monte Carlo simulations of Fig. 2, especially at higher temperatures (lower coverages), is due to the finite lattice which is employed. At low coverages it is less probable that two particles will occupy near-neighbor sites, which is necessary for second-order desorption.

We have investigated the effects of lateral interactions, lattice geometry, and the mobility of the adsorbate on the TPD spectra. The various parameter sets which were employed are listed in Table I. For relatively small lateral interactions, the TPD spectra simulated from Monte Carlo methods and those calculated using the approximate methods outlined above are in good agreement. As lateral interactions are increased, on the other hand, differences between the results also increase. When the interaction is so large that the adsorbate forms an ordered phase, the calculations using statistical approximations cannot even qualitatively reproduce the simulation results.[20,26] We show some typical spectra below using the parameter sets of Table I to stress these effects. In most cases relatively large, but physically realistic, lateral interactions are chosen in order to elucidate the importance of these configurational effects.

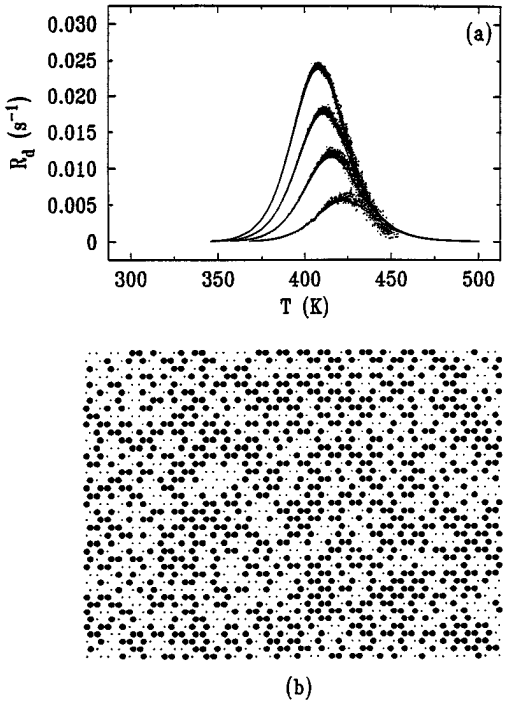

FIG. 2. (a) TPD spectra of recombinative (second-order) desorption generated from Monte Carlo simulations (dots) and the governing continuum equation (solid lines) with initial coverages $\theta_0 = 0.25$, 0.50, 0.75, and 1.00 from bottom to top. (b) A representative configuration at $\theta_A = 0.5$ and $T = 409$ K. These results are generated using parameter set A in Table I on an (80×80) triangular lattice.

TABLE I. Values of parameters used in the simulations. In all cases $E_d(0)$ was taken to be 30 kcal/mol, $k_d^{(0)}$ was taken to be 10^{15} s^{-1}, and, except where noted in the text, the heating rate β was taken to be 1 K/s.

Set	Lattice	E_{nn} (kcal/mol)	E_{nnn} (kcal/mol)
A	Triangular	0.00	0.00
B	Triangular	0.40	0.40
C	Triangular	1.00	0.00
D	Triangular	1.00	0.50
E	Square	1.00	0.00
F	Square	1.00	1.00
G	Square	−0.50	0.00
H	Hexagonal	1.00	0.00
I	Hexagonal	1.00	0.50
J	Square	0.00	0.00

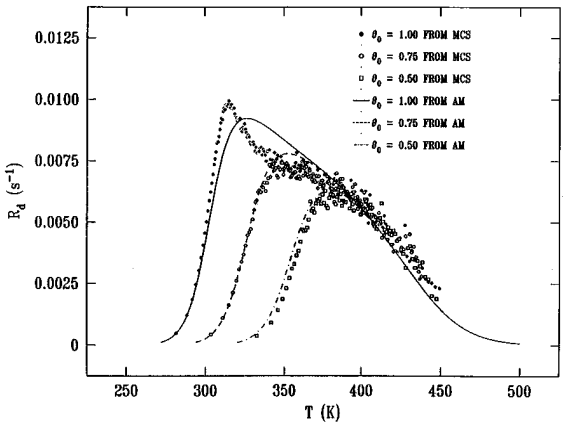

FIG. 3. TPD spectra generated by Monte Carlo simulations (MCS) and approximate methods (AM) using parameter set *B* in Table I on an (80×80) triangular lattice for the indicated initial coverages.

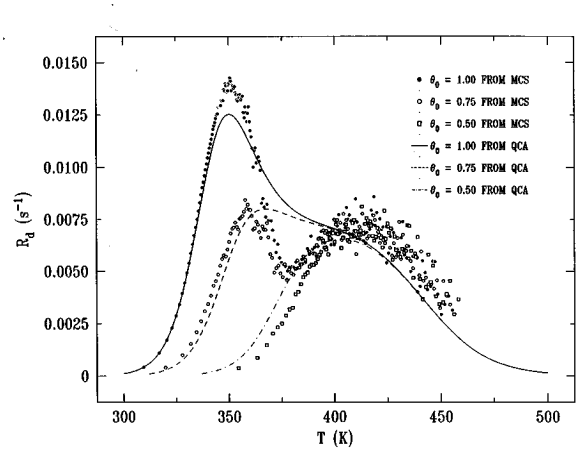

FIG. 4. TPD spectra generated by Monte Carlo simulations (MCS) and the quasichemical approximation (QCA) using parameter set *C* in Table I on an (80×80) triangular lattice for the indicated initial coverages.

A. Triangular lattice

We studied the effects of nearest-neighbor and next-nearest-neighbor interactions on TPD spectra on a triangular lattice using the parameter sets $B-D$ in Table I. Figure 3 shows the TPD spectra on a triangular lattice calculated using Monte Carlo simulations (MCS) and the approximate methods (AM) using parameter set *B* in Table I in which there are weak repulsive nearest-neighbor and next-nearest-neighbor interactions of strength $E_{nn}=E_{nnn}=0.40$ kcal/mol. Compared with Fig. 2, the lateral repulsions result in a downshift of the peak temperatures and a broadening of the peaks. The repulsions also cause, however, the appearance of a rather sharp low-temperature peak in the desorption spectra obtained from Monte Carlo simulations for initial adsorbate coverages greater than 0.75. Although the TPD spectra from the approximate calculations reproduce quantitatively the ones from the Monte Carlo simulations at lower coverages, at higher coverages they only agree qualitatively with the simulation results. For example, the sharp peak in the Monte Carlo simulations is not resolved by the approximate calculations.

Simulations were also performed with different values of the lateral interaction energy to quantify the fact that peak splitting in TPD is a consequence of the lateral repulsions. The TPD spectra with a stronger repulsive nearest-neighbor interaction, $E_{nn}=1.00$ kcal/mol (parameter set *C* in Table I), are shown in Fig. 4. Although, the high-temperature peak intensity and peak position do not vary for initial coverages greater than or equal to 0.50, as the surface coverage increases above 0.50, the intensity of the second, low-temperature peak increases, and its peak position shifts to lower temperature. The initial desorption rate calculated from the quasichemical approximation for $\theta_0=1.0$ is exactly the same as that from Monte Carlo simulations because at saturation coverage all the desorbing pairs have the same local environment and, hence, the same desorption rate. The initial desorption rate from the quasichemical approximation for $\theta_0=0.75$ is lower than that from the Monte Carlo simulations, while the initial desorption rate from the quasichemical approximation for $\theta_0=0.50$ is higher than that from the Monte Carlo simulations. In the quasichemical approximation different pairs of adsorbates are assumed to be independent which underestimates the probabilities of some higher energy configurations for coverages above 1/2 and overestimates the probabilities of some higher energy configurations for coverages less than or equal to 1/2.[20] As a result, the initial desorption rate at higher coverages is lower using the quasichemical approximation, whereas the desorption rate at lower coverages is higher compared with the Monte Carlo simulations. The distinct dip between the two peaks in the Monte Carlo simulations is also smeared out in the statistical approximations. From the adsorbate configurations generated in the Monte Carlo simulations, we know that the system crosses through various ordered phases, and the separation of the two peaks in the Monte Carlo simulations can be easily understood in terms of these adsorbate configurations.[46]

Adding a repulsive next-nearest-neighbor interaction to this repulsive nearest-neighbor interaction results in the appearance of a *significantly* broadened peak for initial surface coverages below 0.75 with a sharp low-temperature peak appearing at an initial surface coverage above 0.75, as deduced from the Monte Carlo simulations. In Fig. 5 we show the simulated TPD spectra with a repulsive nearest-neighbor interaction, $E_{nn}=1.00$ kcal/mol, and a repulsive next-nearest-neighbor interaction, $E_{nnn}=0.50$ kcal/mol (parameter set *D* in Table I). For an initial fractional coverage of unity, we observe two peaks in the simulated TPD spectrum of Fig. 5. The sharp low-temperature peak overlaps with the broad high-temperature peak corresponding to $\theta_0=0.75$ when the fractional surface coverage decreases from unity to about 0.72. For comparison, corresponding results from the approximate methods are also shown in Fig. 5. The low-temperature peak for $\theta_0=1.0$ is only qualitatively reproduced by the approximate methods. The detailed differences between the Monte Carlo simulation results and the approximate calculations are due to the way in which the approximate methods treat the statistics of the lattice, i.e., they consider only one site or two sites.[27,28] Adding larger next-

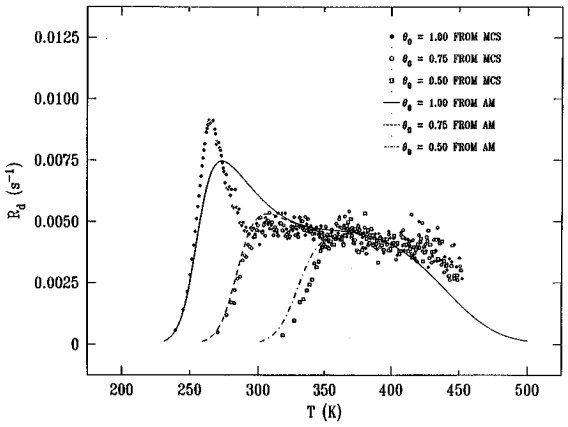

FIG. 5. TPD spectra generated by Monte Carlo simulations (MCS) and approximate methods (AM) using parameter set *D* in Table I on an (80×80) triangular lattice for the indicated initial coverages.

nearest-neighbor repulsions results in further peak splitting of the simulated spectra for initial coverages greater than 0.25.

B. Square lattice

We have also conducted simulations on a square lattice in order to assess the effect of surface geometry on the TPD spectra. Qualitatively similar results have been found for a square lattice as for a triangular lattice for the case of repulsive nearest-neighbor and next-nearest-neighbor interactions. Using the isosteric method of Taylor and Weinberg,[8] we have calculated both the activation energy and the preexponential factor of the desorption rate coefficient for thermal desorption spectra generated using parameter set *E* of Table I. The initial coverage was saturation ($\theta_0=1.0$), and the heating rate was varied from 0.1 to 10 K/s. According to this isosteric analysis the activation energy is given by

$$E_d(\theta_A) = -[\partial \ln(R_d/\theta_A^2)/\partial(k_B T)^{-1}]_{\theta_A}, \tag{11}$$

and the preexponential factor is given by

$$k_d^{(0)}(\theta_A) = \lim_{T\to\infty} R_d/\theta_A^2. \tag{12}$$

The calculated values of E_d and $k_d^{(0)}$ as a function of fractional surface coverage are shown in Figs 6(a) and 6(b), respectively. For fractional coverages near zero, E_d has an approximately constant value of 30 kcal/mol, while $k_d^{(0)}$ is also approximately constant with a magnitude of about 10^{15} s^{-1}. Note that these are precisely the values of E_d and $k_d^{(0)}$ that were put into the simulation for the desorption of isolated pairs of adatoms. At fractional coverages approaching unity, E_d is approximately equal to 24 kcal/mol, and $k_d^{(0)}$ once again approaches 10^{15} s^{-1}. The apparent (''experimentally'' measured) value of E_d goes through a very weak maximum between $\theta_A=0$ and $\theta_A\lesssim 0.5$ and then decreases precipitously to about 25 kcal/mol for $\theta_A\gtrsim 0.5$, cf., Fig. 6(a). Note that the apparent value of E_d *increases* by approximately 2 kcal/mol even though there are only *repulsive* interadsorbate interactions. Likewise, $k_d^{(0)}$ goes through a (more pronounced) maximum at $\theta_A\lesssim 0.5$ (which is between one and two orders

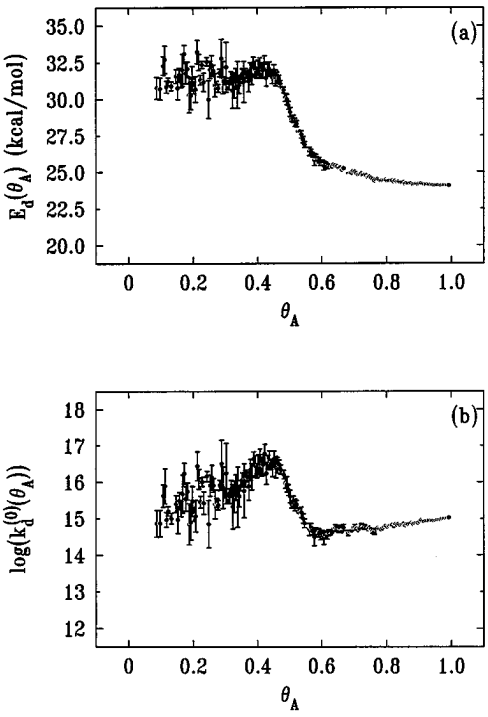

FIG. 6. (a) Activation energy of desorption as a function of coverage. (b) Preexponential factor of the desorption rate coefficient, in units of s^{-1}, as a function of coverage. These results are generated from an isosteric analysis of Monte Carlo simulations on an (80×80) square lattice using parameter set *E* in Table I.

of magnitude greater than its zero-coverage value), decreases to about $10^{14.5}$ s^{-1} for $\theta_A\gtrsim 0.5$, and approaches 10^{15} s^{-1} as $\theta_A\to 1$, cf., Fig. 6(b). This type of behavior has also been found using the quasichemical approximation of variable order parameter,[25] a four-site cluster approximation,[27] the transfer-matrix technique,[21–24] and Monte Carlo simulations[48] of first-order thermal desorption.

The observations of Figs. 6(a) and 6(b) for $\theta_A\lesssim 0.6$ are indicative of a chemical compensation effect, sometimes termed the Meyer–Neldel rule.[49] As discussed in detail elsewhere for the case of a second-order surface reaction,[31] the increase in E_d ($\theta_A\lesssim 0.5$) is due to a temperature dependence of the distribution of local configurations on the surface. Another argument based on the competition between entropy and energy has been given by Kreuzer *et al.*[23,24] The precipitous drop in E_d near a fractional coverage of one-half is due to nearest-neighbor repulsions. At a coverage slightly greater than 0.5, desorption is predominantly from pairs of adsorbates within $c(2\times 2)$ domains, with associated *apparent* rate parameters of $E_d\approx 25$ kcal/mol and $k_d^{(0)}\approx 10^{14.5}$ s^{-1}. For $0.3\lesssim\theta_A\lesssim 0.6$, the compensation effect results in the measurement of *apparent* rate parameters for desorption. For $\theta_A>0.6$, however, we find that E_d and $k_d^{(0)}$ do not vary sympathetically. The decrease in E_d with surface coverage is clearly due to the increasing number of nearest-neighbor pairs, whereas the slight increase of $k_d^{(0)}$ arises from the various distributions of adsorbate configurations at different surface coverages. From Eqs. (1) and (2), we can easily obtain

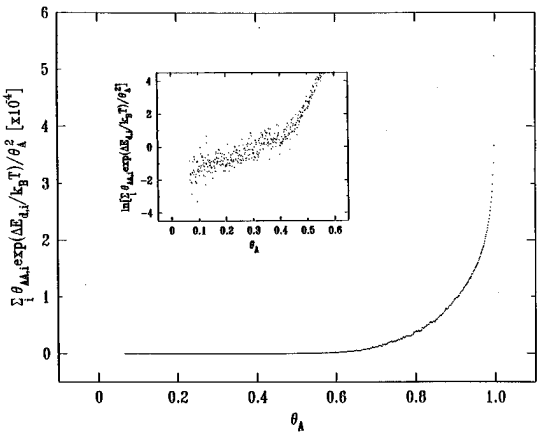

FIG. 7. $\Sigma_i\ \theta_{AA,i}\exp(\Delta E_{d,i}/k_BT)/\theta_A^2$ as a function of surface coverage. The inset is $\ln[\Sigma_i\ \theta_{AA,i}\exp(\Delta E_{d,i}/k_BT)\,\theta_A^2]$ as a function of surface coverage. These results are generated using parameter set E in Table I on an (80×80) square lattice.

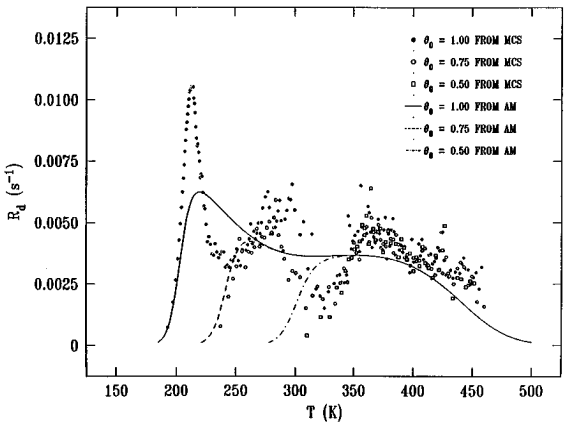

FIG. 8. TPD spectra generated by Monte Carlo simulations (MCS) and approximate methods (AM) using parameter set F in Table I on an (80×80) square lattice for the indicated coverages.

$$K_d^{(0)}(\theta_A)=k_d^{(0)}\exp[E_d(\theta_A)/k_BT]\sum_i\ \theta_{AA,i}\times\exp(-E_{d,i}/k_BT)/\theta_A^2$$

$$=k_d^{(0)}\exp[\Delta E_d(\theta_A)/k_BT]\sum_i\ \theta_{AA,i}\times\exp(\Delta E_{d,i}/k_BT)/\theta_A^2, \tag{13}$$

where

$$\Delta E_{d,i}=N_{\rm nn}(i)E_{\rm nn}+N_{\rm nnn}(i)E_{\rm nnn} \tag{14}$$

and

$$\Delta E_d(\theta_A)=E_d(\theta_A)-E_d(0). \tag{15}$$

Therefore, if

$$\sum_i\ \theta_{AA,i}\exp(\Delta E_{d,i}/k_BT)/\theta_A^2$$

does not vary significantly in the opposite direction of $\Delta E_d(\theta_A)$, we will observe the compensation effect. However, if this ratio changes dramatically in the opposite direction, then the preexponential factor will not vary sympathetically with the change in the activation energy. Indeed, we see a large increase in the ordinate as the surface coverage increases above 0.6 in Fig. 7.

Adding a repulsive next-nearest-neighbor interaction to the repulsive nearest-neighbor interaction results in the occurrence of two peaks in the TPD spectra for an initial fractional surface coverage below 0.75, and three peaks for an initial surface coverage above 0.75. In Fig. 8 we show the simulated TPD spectra with a repulsive nearest-neighbor interaction, $E_{\rm nn}=1.00$ kcal/mol, and a repulsive next-nearest-neighbor interaction, $E_{\rm nnn}=1.00$ kcal/mol (parameter set F in Table I). For an initial fractional coverage of unity, we observe three peaks in the simulated TPD spectrum of Fig. 8. The low-temperature peak near 200 K is quite sharp and is due to a desorbing pair of adatoms which experience a full complement of nearest-neighbor and next-nearest-neighbor repulsions. The peak near 280 K overlaps with the one corresponding to $\theta_0=0.75$ when the fractional surface coverage decreases from unity to about 0.71, and the high-temperature peak near 360 K overlaps with the one corresponding to $\theta_0=0.5$ when the surface coverage decreases to about 0.48. Clearly, the multiple peaks at high coverages cannot be reproduced by the approximate methods, cf., Fig. 8. The difference between the Monte Carlo simulations and the approximate calculations is again due to only one-site and two-site correlations being treated by the approximate methods.[28] The addition of a larger next-nearest-neighbor repulsion can result in better resolution of separate peaks in Monte Carlo simulations, cf., Figs. 5 and 8. In Fig. 9 we show typical configurations at different coverages that are obtained from simulations on an (80×80) square lattice for $\theta_0=1$ with parameters corresponding to the simulated TPD spectra in Fig. 8. Comparing Figs. 8 and 9 provides useful physical insight. The broad high-temperature peak above 325 K, for which $\theta_A<0.5$, is associated with desorption from an ordered (2×1) overlayer $[\theta_A=0.5$, as shown in Fig. 9(b)] to a disordered overlayer at low surface coverage through a weakly ordered (2×2) overlayer $[\theta_A=0.25$, as shown in Fig. 9(a)]. The peak near 280 K, for which $0.5\lesssim\theta_A\lesssim0.75$, is associated with desorption which occurs during a continuous change from an ordered $(2\times2)^*$ overlayer with two adatoms per unit cell $[\theta_A=0.75$, as shown in Fig. 9(c)] to an ordered (2×1) overlayer, cf., Fig. 9(b). The low-temperature peak near 210 K, for which $0.75\lesssim\theta_A\lesssim1.0$, is associated with the recombinative desorption of two adatoms within a local (1×1) environment as the overlayer transforms from this global structure to the $(2\times2)^*$ structure shown in Fig. 9(c).

We have also examined the case of attractive adatom–adatom interactions. Shown in Fig. 10 are both the calculated (via the quasichemical approximation) and simulated TPD spectra with an attractive nearest-neighbor interaction, $E_{\rm nn}=-0.50$ kcal/mol (parameter set G in Table I), on a square lattice. In contrast to the TPD spectra without lateral

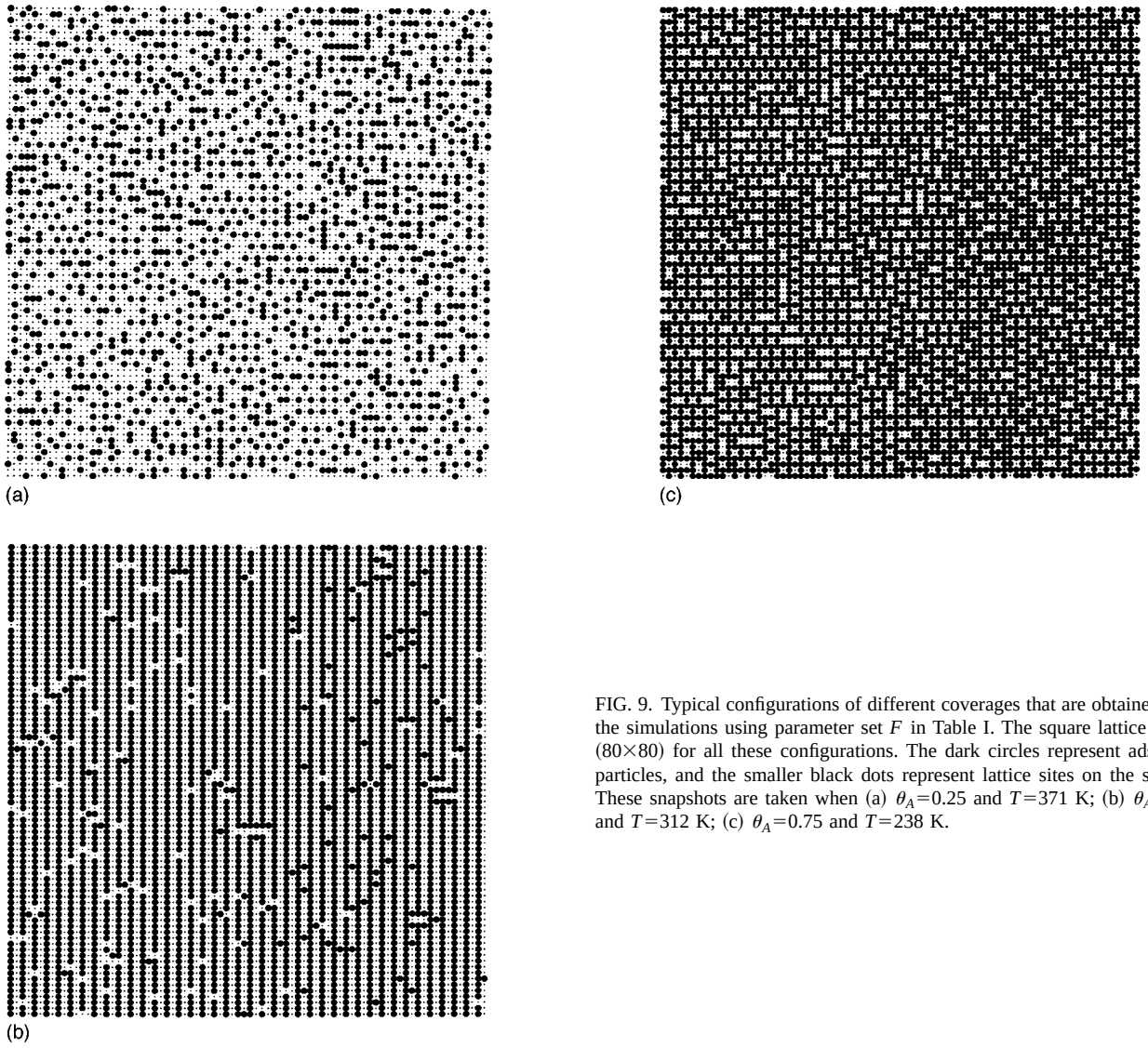

FIG. 9. Typical configurations of different coverages that are obtained from the simulations using parameter set F in Table I. The square lattice size is (80×80) for all these configurations. The dark circles represent adsorbate particles, and the smaller black dots represent lattice sites on the surface. These snapshots are taken when (a) $\theta_A=0.25$ and $T=371$ K; (b) $\theta_A=0.50$ and $T=312$ K; (c) $\theta_A=0.75$ and $T=238$ K.

interactions or with repulsive interactions, attractive interactions cause the peak temperature to shift up with increasing initial coverage. The quasichemical approximation agrees well with the Monte Carlo simulations for low initial coverages. However, as the coverage increases, deviations between the quasichemical calculations and the Monte Carlo simulations become apparent, and the approximately calculated peak temperatures become lower than the simulated ones. Shown in Figs. 11(a) and 11(b) are, respectively, the values of E_d and $k_d^{(0)}$ as a function of fractional surface coverage from Monte Carlo simulations, evaluated using the Taylor–Weinberg method.[8] For fractional coverages close to zero, E_d has an approximate value of 30 kcal/mol, cf., Fig. 11(a); whereas $k_d^{(0)}$ has a value of $10^{15.25}$ s^{-1}, cf., Fig. 11(b). The value of E_d is precisely that which was put into the simulations for the desorption of an isolated pair of admolecules, whereas $k_d^{(0)}$ is slightly higher than the corresponding input value of 10^{15} s^{-1}. At fractional coverages approaching unity, E_d is approximately equal to 33 kcal/mol, which is the activation energy of a desorbing pair of adatoms with all six nearest neighbors occupied $[=E_d(0)-6E_{\rm nn}]$; and k_d^0 approaches 10^{15} s^{-1}, the value which was put into the simulation. For the attractive nearest-neighbor interaction, the ratio

$$\left(\sum_i \theta_{AA,i}\exp(\Delta E_{d,i}/k_BT)\right)\Big/\theta_A^2$$

decreases dramatically as the surface coverage increases, cf., Fig. 12. The ratio is equal to approximately 2.5 in the limit $\theta_A\rightarrow0$, and is equal to 0.0178 in the limit $\theta_A\rightarrow1$, i.e., $[\exp(6E_{\rm nn}/375k_B)]$, cf., inset of Fig. 12.

C. Hexagonal lattice

We have investigated the effect of lateral interactions on TPD spectra on a hexagonal lattice for the case of repulsive adatom–adatom interactions. Figure 13 shows TPD spectra simulated using parameter set H in Table I in which the repulsive nearest-neighbor interaction is $E_{\rm nn}=1.0$ kcal/mol. Unlike the simulations on a triangular lattice (cf., Fig. 4) and a square lattice (not shown but qualitatively similar to Fig. 4), nearest-neighbor repulsions result in the appearance of three peaks for an initial fractional surface coverage of unity and two peaks for $\theta_0=0.66$. Although the sharp peak near 260 K in the Monte Carlo simulations is resolved qualita-

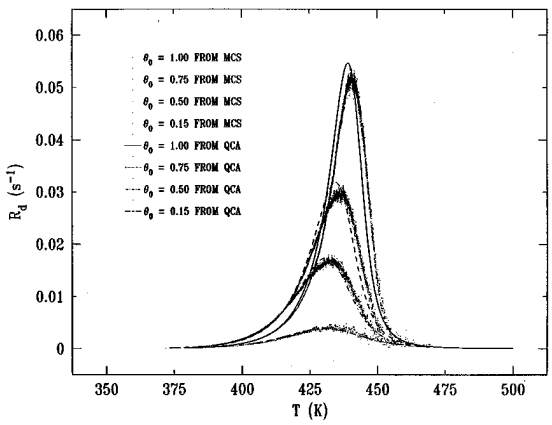

FIG. 10. TPD spectra generated by Monte Carlo simulations (MCS) and the quasichemical approximation (QCA) using parameter set *G* in Table I on an (80×80) hexagonal lattice for the indicated initial coverages.

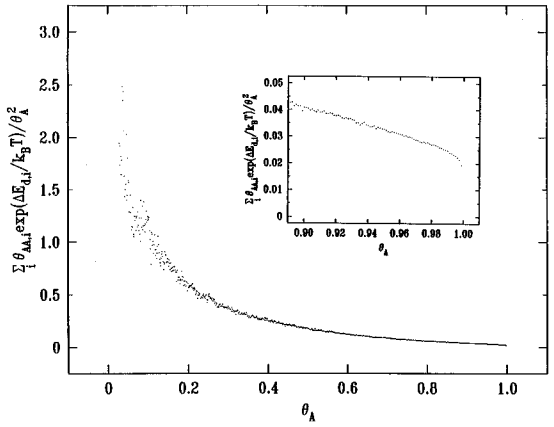

FIG. 12. $\Sigma_i\ \theta_{AA,i}\exp(\Delta E_{d,i}/k_BT)/\theta_A^2$ as a function of surface coverage. These results are generated using parameter set *G* in Table I on an (80×80) square lattice.

tively in the quasichemical calculations, the two higher temperature peaks are not resolved using this approximate methodology. In Fig. 14 we show typical configurations at different coverages that are obtained from the simulations on an (80×80) hexagonal lattice. The three peaks in the simulated TPD spectra of Fig. 13 may be considered in the following way. The low-temperature peak is due to adatoms desorbing from a local (1×1) environment as the structure transforms to a $(\sqrt{3}\times\sqrt{3})^*R30°$ structure with two adatoms per unit cell at $\theta_A=0.67$, cf., Figs. 14(b) and 14(c). The middle peak corresponds to desorption as the overlayer transforms from the $(\sqrt{3}\times\sqrt{3})^*R30°$ structure at $\theta_A=0.67$ to a primitive $(\sqrt{3}\times\sqrt{3})R30°$ structure $\theta_A=0.33$, cf., Figs. 14(a) and 14(b). Finally, the high-temperature peak corresponds largely to desorption from isolated pairs of adatoms as the surface coverage decreases from 0.33 to zero. Inspection of Figs. 14(a) and 14(b) shows there is only limited short-range order in the two $\sqrt{3}$ superstructures during desorption; nevertheless, the above discussion is a useful way to think about the origin of the three peaks in the simulated TPD spectrum corresponding to $\theta_0=1$ in Fig. 13.

Adding repulsive next-nearest-neighbor interactions to the repulsive nearest-neighbor interactions results in the appearance of three peaks for an initial surface coverage below 0.75 and four peaks for initial surface coverages above 0.75. In Fig. 15 we show the simulated TPD spectra with a repul-

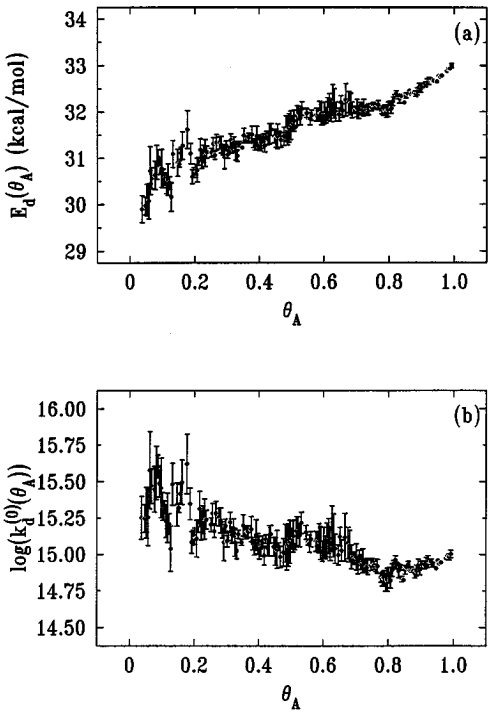

FIG. 11. (a) Activation energy of desorption as a function of coverage. (b) Preexponential factor of the desorption rate coefficient, in units of s^{-1}, as a function of coverage. These results are generated from an isosteric analysis of Monte Carlo simulations on an (80×80) square lattice using parameter set *G* in Table I.

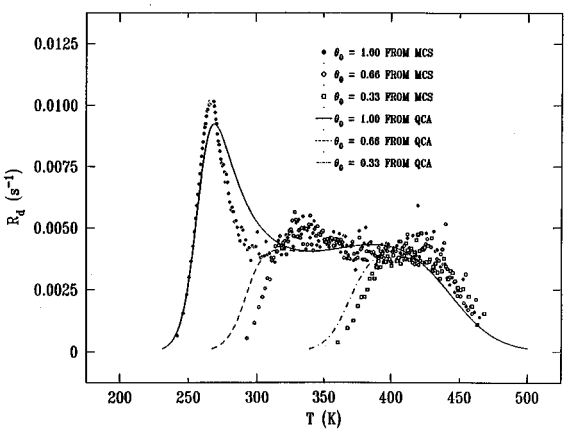

FIG. 13. TPD spectra generated by Monte Carlo simulations (MCS) and the quasichemical approximation (QCA) using parameter set *H* in Table I on an (80×80) hexagonal lattice for the indicated initial coverages.

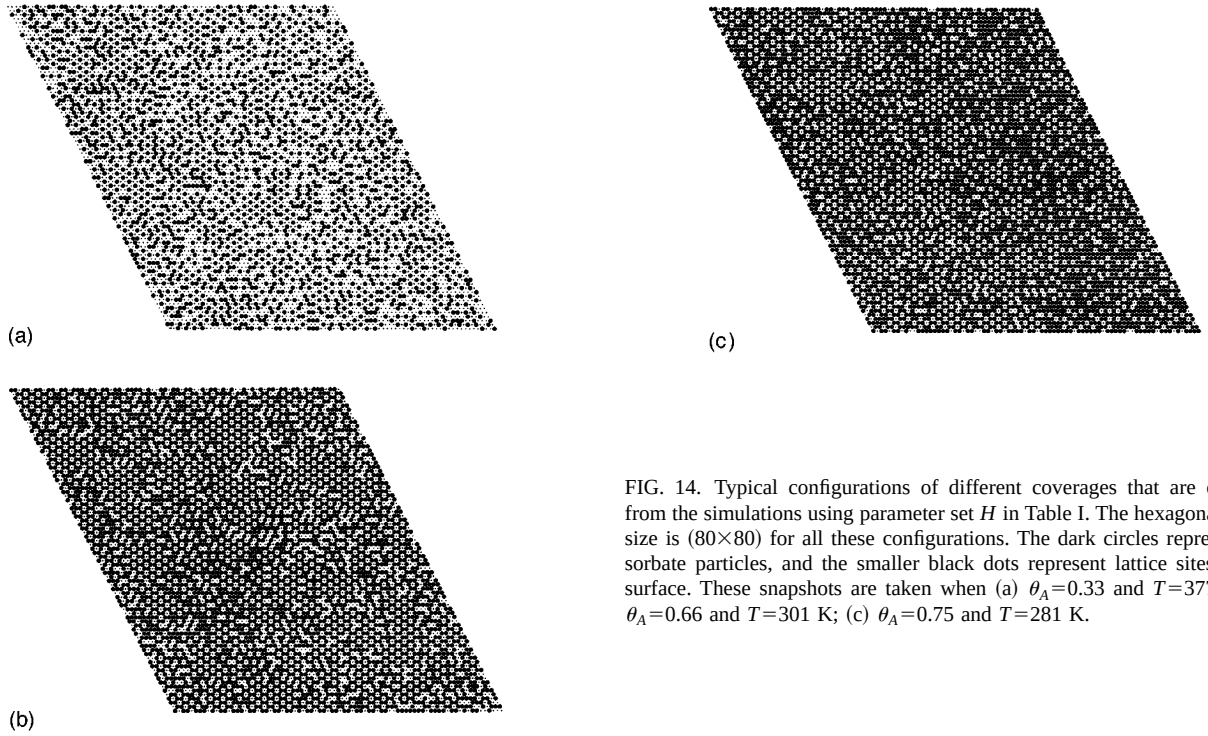

FIG. 14. Typical configurations of different coverages that are obtained from the simulations using parameter set H in Table I. The hexagonal lattice size is (80×80) for all these configurations. The dark circles represent adsorbate particles, and the smaller black dots represent lattice sites on the surface. These snapshots are taken when (a) $\theta_A=0.33$ and $T=377$ K; (b) $\theta_A=0.66$ and $T=301$ K; (c) $\theta_A=0.75$ and $T=281$ K.

sive nearest-neighbor interaction, $E_{nn}=1.0$ kcal/mol, and a repulsive next-nearest-neighbor interaction, $E_{nnn}=0.5$ kcal/mol (parameters set I in Table I). For an initial fractional coverage of unity, the peak near 260 K overlaps with the one corresponding to $\theta_0=0.75$ when the fractional surface coverage decreases from unity to about 0.73, the peak near 325 K overlaps with the one corresponding to $\theta_0=50$ when the surface coverage decreases to about 0.48, and the high-temperature peak near 400 K overlaps with the one corresponding to $\theta_0=0.25$ when the surface coverage decreases to about 0.22. Corresponding results from the approximate calculations qualitatively resolve the low-temperature peak around 180 K for $\theta_0=1.0$. The three higher temperature peaks, however, are not resolved by the approximate calculations. From adsorbate configurations generated from the simulations, we know that the system crosses through various ordered phases [(2×2)*, (2×1), and a weakly ordered (2×2)], and the correlation between the separation of the thermal desorption peaks and the variation of adsorbate configurations is qualitatively the same as the case of repulsive nearest-neighbor and next-nearest-neighbor interactions on a square lattice.

D. Nonequilibrium effects

We have thus far shown the TPD spectra of mobile adsorbates, the diffusion of which is rapid compared to the desorption reaction. In order to understand nonequilibrium effects, it is necessary to consider a finite diffusion rate of the adsorbate compared with the desorption rate. In real systems, the occurrence of this situation might be suggested by TPD spectra which depend on the initial temperature, for example. Here, we investigate the extreme case where diffusion is *completely absent*. Figure 16 shows the TPD spectra obtained from Monte Carlo simulations on a square lattice with an initial fractional coverage of unity using parameter set J in Table I. For comparison, we also show the results obtained using Eq. (1) for first- and second-order desorption, which are exact for systems consisting of randomly distributed adsorbates. In the absence of diffusion, an asymmetric thermal desorption spectrum is obtained, which has the same shape as that of first-order desorption. The fractional coverage of isolated adatoms which remain on the surface after the Monte Carlo simulation of Fig. 16 is the same as the fractional coverage of empty sites from random dimer filling.[50] This can be easily understood from the particle-hole symmetry of the problem, if we consider nonequilibrium associative desorption as time-reversed random dimer filling. As in the random dimer-filling problem, where the jamming coverage depends on the geometry of the lattice, the residual cover-

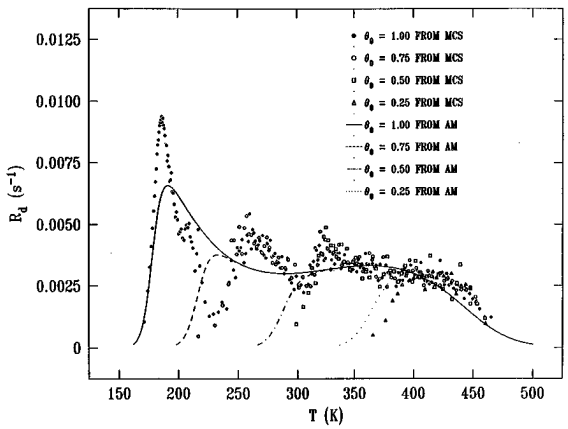

FIG. 15. TPD spectra generated by Monte Carlo simulations (MCS) and approximate methods (AM) using parameter set I in Table I on an (80×80) hexagonal lattice for the indicated initial coverages.

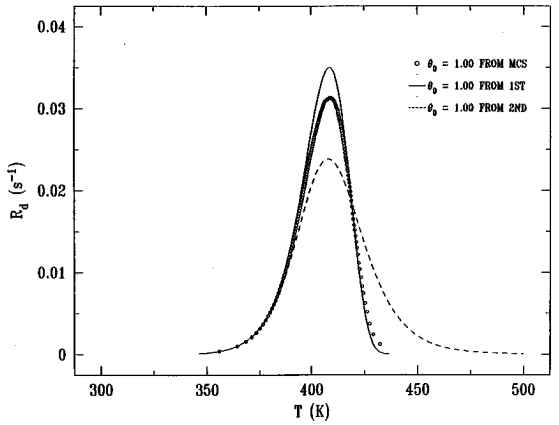

FIG. 16. TPD spectra of an immobile adsorbate generated by Monte Carlo simulations (MCS) and the governing continuum equation for first-order desorption (1st) and second-order desorption (2nd) using parameter set J in Table I on an (80×80) square lattice for an initial fractional surface coverage of unity.

ages after thermal desorption on the triangular, square, and hexagonal lattices are also different. However, the first-order behavior is observed on all three kinds of lattices. For a finite diffusion or relaxation rate, the shape of the desorption spectrum will be between the one with an infinite rate and the one without mobility.

E. Connection to experiment

It is known that more than one set of parameters can lead to good agreement between simulated and experimental TPD spectra. Therefore, unique parameter values cannot be claimed just based on agreement between simulated TPD spectra and experimentally measured ones.[44] Our studies have shown that agreement between the values of $E_d(\theta)$ and $k_d^{(0)}(\theta)$ determined by both experiment and simulation may also be used as criteria for determining the validity of parameters from the simulations. Normally the apparent activation energy and preexponential factor of the desorption rate coefficient measured at very low coverage are close to the actual physical quantities describing the system under study. Therefore, values of $E_d(0)$ and $k_d^{(0)}(0)$ for use in the simulations can be estimated by extrapolating experimental results at low coverages to the limit of zero coverage. The interaction energy (energies) can then be determined variationally to obtain optimal agreement between the simulated results [e.g., TPD spectra, the surface phase diagram, and the coverage-dependent $E_d(\theta)$ and $k_d^0(\theta)$] and the corresponding experimental results.

A proper interpretation of the coverage dependence of desorption spectra in laboratory experiments is complicated not only by adsorbate–adsorbate interactions but also by effects of surface heterogeneity (e.g., different binding sites and surface reconstructions). Therefore, the detailed desorption mechanism cannot be identified by *simply* comparing experimental and calculated TPD spectra. Agreement is a necessary but not sufficient condition for justifying a proposed desorption model. For specific real systems, simulations could also be improved by using more realistic interaction potentials between adsorbates and between the adsorbate and the surface. Independent structural information from experiment is clearly desirable in order to justify a lattice gas treatment. For a nonlattice gas situation, where the binding sites of the adsorbate change with varying coverage, a decorated or embedded lattice of more than one type of adsorption site may be valid.[51–55]

V. SYNOPSIS

We have extended a previously introduced Monte Carlo algorithm to simulate recombinative (second-order) temperature programmed desorption for the case of rapid surface diffusion compared to desorption. We demonstrated the validity of the algorithm by investigating overlayers without adsorbate–adsorbate interactions and showed that the simulated TPD spectra correspond to those calculated from the proper continuum master equation. We also demonstrated that multiple peaks in recombinative TPD spectra of interacting adsorbates are correlated with transitions between adsorbate configurations on the surface. The separation between the peak temperatures is strongly dependent on the strength and nature of the lateral interactions. Larger repulsive interactions typically result in greater separation (and hence, resolution) of the desorption peaks. Smaller repulsions result in less peak separation and, possibly, single peak broadening rather than peak splitting. Attractive interactions result in an upshift and sharpening of the desorption peaks. All of these observations can be understood in terms of the distribution of local surface configurations. For relatively small lateral interactions, the TPD spectra generated from Monte Carlo simulations and approximate methods (quasichemical and mean field) are in good agreement. However, as the lateral interactions are increased, differences between the simulation and calculated results also increase. When the interaction is so large that the adsorbate forms an ordered phase at the desorption temperature, the calculations using approximate methods cannot even qualitatively reproduce the Monte Carlo simulation results, e.g., multiple peaks in the TPD spectrum.

We have also examined the coverage dependence of the activation energy and preexponential factor of the desorption rate coefficient for two different cases, namely, repulsive and attractive nearest-neighbor interactions on a square lattice. We have shown that the preexponential factor $k_d^{(0)}(\theta_A)$ can be expressed as

$$k_d^{(0)} \exp[\Delta E_d(\theta_A)/k_BT]\sum_i \theta_{AA,i} \exp(\Delta E_{d,i}/k_BT)/\theta_A^2.$$

Therefore, if the ratio

$$\sum_i \theta_{AA,i} \exp(\Delta E_{d,i}/k_BT)/\theta_A^2$$

does not vary significantly in the opposite direction of the variation in the activation energy $\Delta E_d(\theta_A)$, the preexponential factor and the activation energy will both vary, but in a way that compensate each one's individual variation insofar as the overall rate is concerned. However, if the ratio

changes dramatically in the opposite direction, then the preexponential factor will not vary sympathetically with the change in the activation energy. We elucidated the kinetic compensation effect by calculating the ratio

$$\sum_i \theta_{AA,i} \exp(\Delta E_{d,i}/k_B T)/\theta_A^2.$$

For repulsive nearest-neighbor interactions, we found that the ratio does not vary significantly in the opposite direction of $\Delta E_d(\theta_A)$ for $\theta_A \lesssim 0.6$, and the activation energy and preexponential factor vary sympathetically with coverage, showing a kinetic compensation effect. However, as surface coverage increases above 0.6, the ratio increases dramatically while the activation energy decreases, and the preexponential factor does not vary sympathetically with the activation energy. For attractive nearest-neighbor interactions, on the other hand, the ratio decreases dramatically for $\theta_A \lesssim 0.8$, while the activation energy increases, and the preexponential factor and the activation energy do not vary sympathetically. However, for $\theta_A \gtrsim 0.8$, the ratio varies slightly, and we observed the compensation effect in the activation energy and preexponential factor of the desorption rate coefficient. These observations support our earlier assertion[31] that kinetic compensation results from a varying distribution of local adatom configurations as a function of surface coverage and temperature. Finally, we investigated the case of an immobile adsorbate overlayer. For the case of no lateral interactions, the thermal desorption spectrum has the characteristic shape of first-order thermal desorption. Both this result and the observed coverage can be explained from the particle-hole symmetry of its time-reversed process, namely, nonequilibrium random dimer filling of a surface.

ACKNOWLEDGMENT

We gratefully acknowledge the financial support of the National Science Foundation (Grant No. CHE-9300020).

[1] P. A. Redhead, Vacuum **12**, 203 (1962).
[2] A. M. de Jong and J. W. Niemantsverdriet, Surf. Sci. **233**, 355 (1990).
[3] E. Tronconi and L. Lietti, Surf. Sci. **199**, 43 (1988).
[4] D. A. King, T. E. Madey, and J. T. Yates, J. Chem. Phys. **55**, 3236 (1971).
[5] E. Bauer, H. Poppa, G. Todd, and F. Bonczek, J. Appl. Phys. **45**, 5164 (1974).
[6] J. L. Falconer and R. J. Madix, J. Catal. **48**, 262 (1977).
[7] C. M. Chan, R. Aris, and W. H. Weinberg, Appl. Surf. Sci. **1**, 360 (1978).
[8] J. L. Taylor and W. H. Weinberg, Surf. Sci. **78**, 259 (1978).
[9] V. P. Zhdanov, Surf. Sci. Rep. **12**, 183 (1991), and references therein; A. C. F. Kong and L. D. Schmidt, Surf. Sci. **193**, 417 (1988), and references therein.
[10] R. J. Baxter, *Exact Solved Models in Statistical Mechanics* (Academic, London, 1982).
[11] A. Córdoba and J. J. Luque, Phys. Rev. B **26**, 4028 (1982).
[12] V. P. Zhdanov, Surf. Sci. **102**, L35 (1981); **111**, L662 (1981); **123**, 106 (1983); **133**, 469 (1984); **137**, 515 (1986); **169**, 1 (1986); **179**, L57 (1987).
[13] B. Hellsing and V. P. Zhdanov, Chem. Phys. Lett. **147**, 613 (1988).
[14] H. J. Kreuzer and H. S. Payne, Surf. Sci. **198**, 235 (1988); **200**, L433 (1988); **205**, 153 (1988); **222**, 404 (1989).
[15] J. B. Benziger and G. R. Schoofs, J. Phys. Chem. **88**, 4439 (1984).
[16] S. Sundaresan and K. R. Kaza, Surf. Sci. **160**, 103 (1985); Chem. Eng. Commun. **32**, 333 (1985); **35**, 1 (1985).
[17] H. Asada and M. Masuda, Surf. Sci. **207**, 517 (1989).
[18] A. Surda and I. Karasova, Surf. Sci. **109**, 605 (1981).
[19] A. Surda, Surf. Sci. **220**, 295 (1989).
[20] J. L. Sales, G. Zgrablich, and V. P. Zhdanov, Surf. Sci. **209**, 208 (1989).
[21] A. V. Myshlyavtsev and V. P. Zhdanov, Chem. Phys. Lett. **162**, 43 (1989).
[22] A. V. Myshlyavtsev, J. L. Sales, G. Zgrablich, and V. P. Zhdanov, J. Stat. Phys. **58**, 1029 (1990).
[23] S. H. Payne, H. J. Kreuzer, and L. D. Roelofs, Surf. Sci. Lett. **259**, L781 (1991).
[24] S. H. Payne, J. Zhang, and H. J. Kreuzer, Surf. Sci. **246**, 185 (1992).
[25] H. Pak and J. W. Evans, Surf. Sci. **186**, 550 (1987).
[26] J. W. Evans, K. K. Hoffman, and H. Pak, Surf. Sci. **192**, 475 (1987).
[27] A. Wierzbicki and H. J. Kreuzer, Surf. Sci. **257**, 417 (1991).
[28] H. J. Kreuzer, Langmuir **8**, 774 (1992).
[29] E. S. Hood, B. H. Toby, and W. H. Weinberg, Phys. Rev. Lett. **55**, 2437 (1985).
[30] W. H. Weinberg, in *Kinetics of Interface Reactions*, Vol. 8 of *Springer Series in Surface Science*, edited by M. Grunze and H. J. Kreuzer (Springer, Berlin, 1987), pp. 94–125.
[31] H. C. Kang, T. A. Jachimowski, and W. H. Weinberg, J. Chem. Phys. **93**, 1418 (1990).
[32] K. A. Fichthorn and W. H. Weinberg, Langmuir **7**, 2539 (1991).
[33] H. C. Kang and W. H. Weinberg, Acc. Chem. Res. **25**, 253 (1992).
[34] R. M. Lambert and M. E. Bridge, Proc. R. Soc. London, Ser. A **370**, 545 (1980); Surf. Sci. **94**, 469 (1980).
[35] M. Silverberg and A. Ben-Shaul, Chem. Phys. Lett. **134**, 491 (1987); J. Chem. Phys. **87**, 3178 (1987); J. Stat. Phys. **52**, 1179 (1988); Surf. Sci. **214**, 17 (1989).
[36] M. Stiles and H. Metiu, Chem. Phys. Lett. **128**, 337 (1986).
[37] D. Gupta and C. S. Hirtzel, Chem. Phys. Lett. **149**, 527 (1988); Surf. Sci. **210**, 322 (1989); Mol. Phys. **68**, 583 (1989).
[38] J. W. Evans and H. Pak, Surf. Sci. **199**, 28 (1988).
[39] S. J. Lombardo and A. T. Bell, Surf. Sci. **206**, 101 (1988); **224**, 451 (1989); Surf. Sci. Rep. **13**, 1 (1991).
[40] J. L. Sales and G. Zgablich, Surf. Sci. **187**, 1 (1987); Phys. Rev. B **35**, 9520 (1987).
[41] J. L. Sales, G. Zgrablich, and V. P. Zhdanov, Surf. Sci. **209**, 208 (1989).
[42] L. V. Lutsevich, O. A. Tkachenko, and V. P. Zhdanov, Langmuir **7**, 1225 (1991); **8**, 1757 (1992).
[43] J. M. Heras, A. P. Velasco, L. Viscido, and G. Zgrablich, Langmuir **7**, 1124 (1991).
[44] K. Nagai and K. H. Bennemann, Surf. Sci. **260**, 286 (1992).
[45] W. H. Weinberg, in *Dynamics of Gas-Surface Interactions*, edited by C. T. Rettner and M. N. R. Ashfold (Royal Society of Chemistry, Cambridge, 1991) pp. 171–220.
[46] B. Meng and W. H. Weinberg, J. Chem. Phys. **100**, 5280 (1994).
[47] D. Menzel, in *Kinetics of Interface Reactions*, Ref. 30, pp. 2–18.
[48] K. A. Fichthorn and W. H. Weinberg, J. Chem. Phys. **95**, 1090 (1991).
[49] W. Meyer and H. Neldel, Z. Tech. Phys. **18**, 588 (1937).
[50] R. S. Nord and J. W. Evans, J. Chem. Phys. **82**, 2795 (1985).
[51] E. Schweizer, B. N. J. Persson, M. Tushaus, D. Hoge, and A. M. Bradshaw, Surf. Sci. **213**, 49 (1989).
[52] B. N. J. Persson, Phys. Rev. B **40**, 7115 (1989); B. N. J. Persson, M. Tushaus, and A. M. Bradshaw, J. Chem. Phys. **92**, 5013 (1990).
[53] A. V. Myshlyavtsev and V. P. Zhdanov, Langmuir **9**, 1290 (1993); V. P. Zhdanov, Surf. Sci. **277**, 155 (1992); V. Bustos, G. Zhrablich, and V. P. Zhdanov, Appl. Phys. A **56**, 73 (1993).
[54] C. Uebing, Surf. Sci. **272**, 247 (1992).
[55] A. R. Cuesta and G. Zgrablich, Surf. Sci. **275**, L636 (1992).